

01 Jan 1990

## SANS From Tetradecylpyridinium Bromide Based Microemulsions

Paul M. Lindemuth

Boualem Hammouda

Raymond L. Venable

*Missouri University of Science and Technology*

Follow this and additional works at: [https://scholarsmine.mst.edu/chem\\_facwork](https://scholarsmine.mst.edu/chem_facwork)

 Part of the [Chemistry Commons](#)

---

### Recommended Citation

P. M. Lindemuth et al., "SANS From Tetradecylpyridinium Bromide Based Microemulsions," *Journal of Physical Chemistry*, vol. 94, no. 21, pp. 8247 - 8250, American Chemical Society, Jan 1990.

The definitive version is available at <https://doi.org/10.1021/j100384a049>

This Article - Journal is brought to you for free and open access by Scholars' Mine. It has been accepted for inclusion in Chemistry Faculty Research & Creative Works by an authorized administrator of Scholars' Mine. This work is protected by U. S. Copyright Law. Unauthorized use including reproduction for redistribution requires the permission of the copyright holder. For more information, please contact [scholarsmine@mst.edu](mailto:scholarsmine@mst.edu).

# SANS from Tetradecylpyridinium Bromide Based Microemulsions

Paul M. Lindemuth,\*

Department of Chemistry, University of Missouri—Rolla, Rolla, Missouri 65401

Boualem Hammouda,†

Research Reactor Facility, University of Missouri—Columbia, Research Park, Columbia, Missouri 65211

and Raymond L. Venable

Department of Chemistry, University of Missouri—Rolla, Rolla, Missouri 65401

(Received: December 28, 1989; In Final Form: April 13, 1990)

Small-angle neutron scattering is used to investigate tetradecylpyridinium bromide/pentanol/heptane/heavy water microemulsions in the water-in-oil (W/O) microemulsion phase diagram region. The heavy water content is increased while the other components (surfactant, cosurfactant, hydrocarbon) are kept constant. With use of a simple model assuming spherical micelles interacting with a hard-sphere potential (Percus-Yevick model), aggregate sizes and packing fractions have been extracted and found to agree with values determined from the mixing conditions. These experiments clearly show the transition from the single-particle (heavy water + Stern layer droplet) scattering regime at low water concentration to the mixed single/interdroplet scattering regime when the intermicellar distance becomes comparable to the size of the micelles.

## Introduction

Since their inception in 1943 by Hoar and Schulman,<sup>1</sup> microemulsions have been the subject of a considerable number of investigations. The term microemulsion is generally used to refer to thermodynamically stable, optically transparent mixtures of water, hydrocarbon, surfactant, and sometimes cosurfactant that form spontaneously upon mixing. Recent review articles<sup>2-4</sup> exist in the literature.

Small-angle neutron scattering (SANS) is a useful diagnostic technique to investigate the morphology of microemulsion systems. A computerized literature search of the Chemical Abstracts Service data base using "neutron" and "micelle" as keywords has retrieved over 100 publications since 1975. Only a few recent reviews are referenced here.<sup>5-7</sup> Deuteration of one of the components (either the hydrocarbon in normal micelles or the water in inverted micelles) enhances the contrast offered to neutrons and therefore the sensitivity in extracting average droplet sizes and interactions.<sup>5,8-11</sup> The contrast can also be adjusted through deuterated/protonated component mixtures to specified levels so as to observe, for example, the micellar shell (the Stern layer) region. Specific deuteration of the heads or the tails of the surfactant molecules has also been applied<sup>11</sup> to obtain the density distribution of these deuterated portions within the micellar system. SANS spectra from partially deuterated micellar systems show either a decreasing dependence on the scattering vector  $Q$  for low droplet concentrations or a broadly peaked behavior when interdroplet contributions are large. Micellar droplets are usually modeled<sup>11</sup> by spherical or ellipsoidal shapes while interdroplet interactions have been described<sup>8</sup> by using typical models such as the mean spherical approximation or its special case (in the zero charge limit), the Percus-Yevick model. The SANS technique can give information pertaining to polydispersity only indirectly. One can incorporate polydispersity into a particular model, as per Sheu and Chen,<sup>12</sup> and extract some secondary information. In the present work, we have used a simplified model (hard spheres) and given no assumptions or treatment concerning effects such as polydispersity or Coulombic interactions.

Studies of phase equilibria by Venable<sup>13</sup> have shown that systems using tetradecylpyridinium bromide (TPB) as surfactant and alcohols as cosurfactant are more effective at solubilizing water

TABLE I: Sample Mixing Conditions

sample ID	TPB, wt %	heptane, wt %	pentanol, wt %	D <sub>2</sub> O, wt %	H <sub>2</sub> O, wt %
TPB1	12.8	69.4	12.3	5.5	0.0
TPB2	12.8	69.8	12.3	0.0	5.0
TPB3	11.9	64.8	11.4	11.8	0.0
TPB4	12.0	65.3	11.5	0.0	11.2
TPB5	11.0	59.8	10.5	18.6	0.0
TPB6	11.2	61.0	10.7	0.0	17.1
TPB7	9.3	55.2	9.7	24.9	0.0
TPB8	10.4	56.6	10.0	0.0	23.0

than the analogous systems employing sodium dodecyl sulfate (SDS) as surfactant. Pyridinium salts were also shown to have a higher water-solubilizing capacity than the corresponding trimethyl salts, perhaps due to the greater solubility of aromatics in water. Similar results<sup>14</sup> were obtained for SDS with medium-chain-length amines as cosurfactant; the increased solubility is presumably due to the ability of the cosurfactant to shield the head-group charge repulsion of the surfactant.<sup>15</sup> The resulting enhancement of the W/O microemulsion solubility area (denoted  $L_2$ ) at high oil content with TPB as surfactant provides the opportunity to probe for structural transitions over a relatively large area of the phase diagram. The aim of the present study is to gain information pertaining to the surfactant assemblies through

(1) Hoar, T. H.; Schulman, J. H. *Nature (London)* **1943**, *152*, 102.

(2) Friberg, S. E.; Venable, R. L. *Encyclopedia of Emulsion Technology*; Dekker: New York, 1983; Vol. 1, p 287.

(3) Gillberg, G. *Emulsions and Emulsion Technology*; Dekker: New York, 1984; Vol. 6, p 1.

(4) Tadros, T. F. *Surfactants in Solution*; Plenum Press: New York, 1984; Vol. 3, p 1501.

(5) Cabane, B. *Surf. Sci. Ser.* **1987**, *22*, 57.

(6) Zemb, T.; Charpin, P. *Surfactants in Solution*; Plenum Press: New York, 1986; Vol. 4, p 141.

(7) Hayter, J.; Penfold, J. *Mol. Phys.* **1981**, *42*, 109.

(8) Hayter, J. B. *Proc. Int. Sch. Phys.* **1985**, *90*, 59.

(9) Chen, S. H. *Physica (B + C)* **1986**, *137*, 183.

(10) Magid, L. J. *Colloids Surf.* **1986**, *19*, 129.

(11) Chen, S. H. *Ann. Rev. Phys. Chem.* **1987**, *47*, 351.

(12) Shew; Chen.

(13) Venable, R. L. *J. Am. Oil Chem. Soc.* **1985**, *62*, 1.

(14) Venable, R. L.; Elders, K. L.; Fang, J. J. *Colloid Interface Sci.* **1986**, *109*, 130.

(15) Nguyen, D. T. Ph.D. Thesis; University of Missouri—Rolla: Rolla, MO, 1988; Chapters 2-3.

\* To whom correspondence should be addressed.

† Present address: Materials Science and Engineering Laboratory, Building 235, E121, National Institute of Standards & Technology, Gaithersburg, MD 20899.

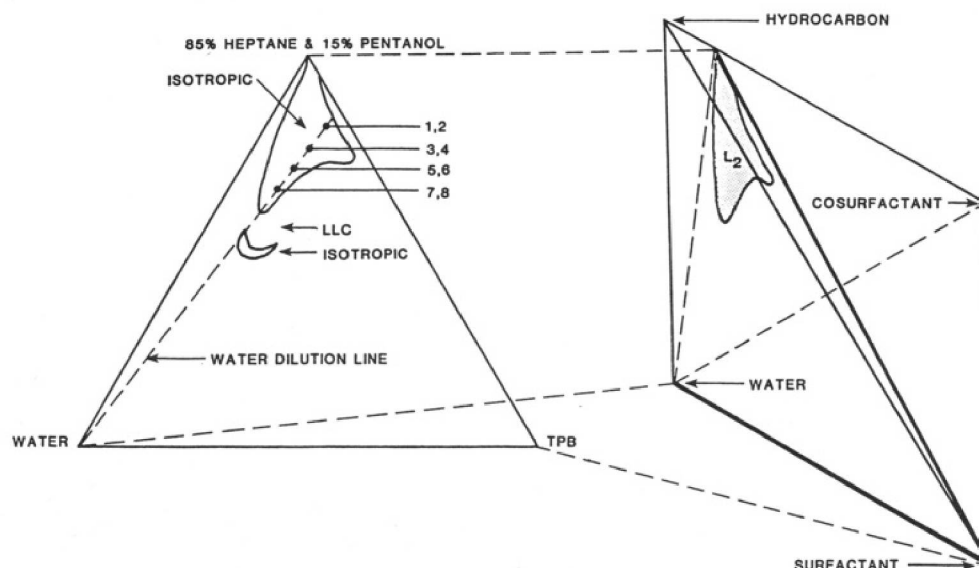


**Figure 1.** Location of the four samples used in the SANS experiments on the phase diagram of this microemulsion system.

direct measurement in a chemical system for which boundaries of the  $L_2$  and middle phases have already been established.

### Experiments

Tetradecylpyridinium bromide (TPB) is a cationic surfactant that forms microemulsions only in the presence of a cosurfactant (usually a medium-chain-length alcohol). The pseudoternary phase diagram<sup>13,16</sup> for the TPB–85% heptane/15% pentanol–water system was generated via the observation of clear to turbid titrimetric end points. Nonbirefringent to birefringent transitions were used to delineate the demixing line in the proximity of the lamellar liquid crystal (LLC) region. The resulting pseudoternary phase diagram is shown in Figure 1 along with its depiction as a plane in a tetrahedral quaternary phase diagram. The region denoted LLC refers to an undelineated region containing single-phase LLCs and two-phase compositions containing LLCs.

TPB was synthesized<sup>12</sup> by refluxing 30 mol % excess freshly distilled pyridine with tetradecyl bromide in methanol solution. The methanol was partially distilled away, and diethyl ether was added until precipitation of the surfactant was initiated. Precipitation was completed in an ice bath. The product was filtered cold and recrystallized six times by dissolving in a minimal amount of methanol and adding ether as described above. Water was doubly distilled from an acidic permanganate solution in an all-glass system. The heptane and pentanol were purchased (and used as received) from the Fischer Scientific Co. Deuterium oxide (99.8 atom % D) was purchased (and used as received) from the Aldrich Chemical Co.

A set of four samples containing TPB as surfactant, pentanol as cosurfactant, heptane, and heavy water in the relative concentrations reported in Table I (TPB1, 3, 5, 7) were prepared. Another set of four “blank” samples (TPB2, 4, 6, 8) containing nondeuterated water were prepared by using the same mole fractions of all components. The locations of the samples are shown on the phase diagram in Figure 1. Each sample in these two sets was prepared by first weighing dry surfactant into a screw-cap culture tube. A solution of 85% heptane and 15% pentanol was then added dropwise in an amount necessary to obtain the desired starting point for titration. These solutions were titrated with heavy water (or normal water for blank samples) and vigorously stirred on a vortex mixer until the desired water content on the water dilution line (see Figure 1) was reached. Water weight fractions ranged from 5.0% to 23.0%, hence covering the realm of closed structures and omitting regions of premicellar aggregates<sup>17,18</sup> and bicontinuous structures<sup>19,20</sup> as suggested by

PGSE-NMR measurements reported elsewhere.<sup>16</sup> After preparation, samples were subsequently transferred to 2-mm-path-length cylindrical quartz cells specifically designed for SANS measurements. The cells were sealed with tight-fitting Teflon stoppers.

SANS data were taken at the University of Missouri Research Reactor Facility with the usual instrument configuration:<sup>21</sup> matched sample-to-detector distances of 450 cm, a wavelength of 4.75 Å (yielding a scattering wavenumber in the range of  $0.008 \text{ \AA}^{-1} < Q < 0.09 \text{ \AA}^{-1}$ ), and source and sample apertures of 2 and 1 cm, respectively. Seven-hour runs were taken from the TPB samples and from an empty quartz cell to correct for background scattering. Two of these samples (TPB7, 8) were also measured in 1-mm-thick cells to check the amount of multiple scattering. No apparent difference between the two thicknesses was observed.

### Treatment of the SANS Data

Since the nondeuterated samples did not show a coherent ( $Q$ -dependent) signal, the following sample blank and background corrections have been performed to extract the coherent part ( $I_{\text{coh}}(Q)$ ) of the scattered intensity from the partially deuterated samples:

$$I_{\text{coh}}(Q) = [I_{d/h}(Q)/T_{d/h}] - I_{\text{eqc}} - \left( \frac{\sum_w^i}{\sum_{\text{tot}}^i} \right) [I_h(Q)/T_h] - I_{\text{eqc}} \quad (1)$$

where  $I_{d/h}$ ,  $I_h$ , and  $I_{\text{eqc}}$  are measured intensities from the partially deuterated and nondeuterated samples and from the empty quartz cell, while the  $T$ 's are the corresponding sample transmissions. The scaling factor ( $\sum_w^i / \sum_{\text{tot}}^i$ ) is the ratio of the incoherent macroscopic cross sections for the water fraction and for the whole (nondeuterated) sample. These ratios are calculated to be 4.1%, 10.8%, 13.6%, and 18.5% for the four samples (TPB2, 4, 6, 8). The data files resulting from blank/background correction were denoted TPB12, 34, 56, 78.

### Intradroplet/Interdroplet Structure Factors

The scattered intensity for a droplet system of arbitrary concentration is in general given by the expression

$$I(Q) = P_{11}(Q) + (N/V) \int d\mathbf{R}_{12} \exp(i\mathbf{Q} \cdot \mathbf{R}_{12}) g_{\text{cm}}(R_{12}) P_{12}^{\text{cond}}(Q) \quad (2)$$

(18) Friberg, S. E.; Flaim, T. D.; Plummer, P. L. *Macro- and Microemulsions*; American Chemical Society: Washington, DC, 1985.

(19) Blum, F. D.; Pickup, S.; Ninham, B. W.; Chen, S. J.; Evans, D. F. *J. Phys. Chem.* **1985**, *89*, 711.

(20) Scriven, L. E. *Micellization, Solubilization and Microemulsions*; Plenum Press: New York, 1977; Vol. 2, p 877.

(21) Mildner, D. F. R.; Berliner, R.; Pringle, O. A.; King, S. J. *J. Appl. Crystallogr.* **1981**, *14*, 370.

(16) Lindemuth, P. M.; Duke, J. R.; Blum, F. D.; Venable, R. L. *J. Colloid Interface Sci.* **1990**, *135*, 539.

(17) Sjolom, E.; Friberg, S. E. *J. Colloid Interface Sci.* **1978**, *67*, 16.

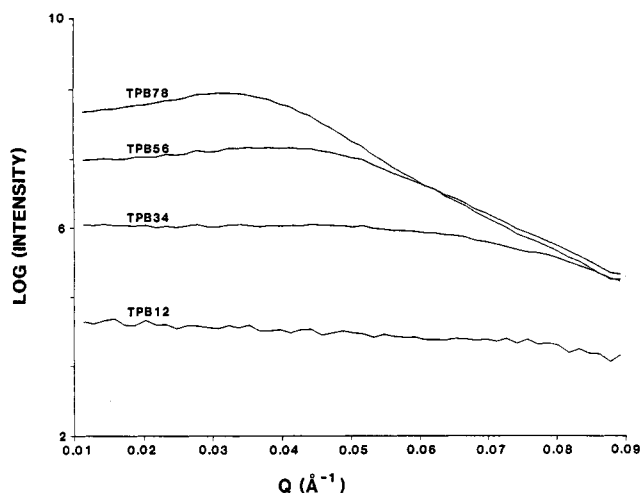


Figure 2. SANS spectra from TPB/pentanol/heptane/heavy water microemulsions for various relative concentrations. Intensities are plotted on an arbitrary logarithmic scale.

where angular correlations (important only in the liquid-crystalline phase) are present. This formula uses an interdroplet pair correlation function  $g_{cm}(R)$  and two intradroplet structure factors:

$$P_{11}(Q) = (1/n) \langle \rho_1(-Q) \rho_1(Q) \rangle \quad (3a)$$

$$P_{12}(Q) = (1/n) \langle \rho_1(-Q) \rho_2(Q) \rangle_{\text{cond}} \quad (3b)$$

Here  $N$ ,  $n$ , and  $V$  are the total number of droplets, number of particles per droplet (heavy water + head groups in the Stern layer), and the total sample volume, while  $\rho_\alpha(Q)$  is the fluctuating density associated with droplet  $\alpha$ . Note that the machine constant containing aperture and flux consideration has been omitted so that relative intensities are being considered. The last ensemble average  $\langle \dots \rangle_{\text{cond}}$  is a configuration average over two droplets (here referred to as 1 and 2) separated by an interdistance (center-to-center)  $R_{12}$ . In the general case, this conditional average depends on  $R_{12}$ . In the special case where orientational correlations are not important (such as in the isotropic phase being investigated here), the integral term can be split as a product of interdroplet and intradroplet contributions giving a simpler (more common) form:

$$I(Q) = P(Q) + nP(Q) h_{cm}(Q) \quad (4a)$$

$$= P(Q) S_{cm}(Q) \quad (4b)$$

in terms of the single droplet structure factor  $P(Q)$  and the interdroplet (here referred to as c-of-m) structure factor  $S_{cm}(Q)$ .  $h_{cm}(Q)$  is the total correlation function, which is expressed in terms of the direct correlation function  $C_{cm}(Q)$  by the Ornstein-Zernicke form:

$$h_{cm}(Q) = C_{cm}(Q) / [1 - nC_{cm}(Q)] \quad (4c)$$

Since there is PGSE-NMR evidence<sup>16</sup> that our samples are characterized by spherical droplets, this last formalism (eqs 4) was used to analyze SANS data.

$P(Q)$  was modeled by the usual structure factor for a sphere of radius  $R$ ,  $[3j_1(QR)/QR]^2$ , where  $j_1(QR)$  is the spherical Bessel function of first order, while  $C_{cm}(Q)$  is borrowed from the Percus-Yevick model with hard-sphere potential. Such an approach has the advantage of making use of compact analytical forms for fitting the data with two floating parameters (sphere radius  $R$  and packing fraction  $\eta$ ). This treatment is a special case of the mean sphere approximation model,<sup>7</sup> which uses two more parameters (interaction strength and range) besides  $R$  and  $\eta$ .

## Results and Discussion

As Figure 2 shows, the SANS spectrum for the lowest water content shows a slowly decreasing variation while the others are characterized by a broad peak. The decreasing dependence of

TABLE II: Moieties and Scattering Lengths

moiety	mol wt	est vol, nm <sup>3</sup>	scattering length, 10 <sup>-12</sup> cm
CH <sub>2</sub>	14.0	0.0262	-0.0834
CH <sub>3</sub>	15.0	0.0517	-0.4567
pyridinium head group	79.0	0.0364	2.394
Br <sup>-</sup>	79.9	0.0517	0.679
H <sub>2</sub> O	18.0	0.0299	-0.168
D <sub>2</sub> O	20.0	0.0301	1.916
C <sub>8</sub> H <sub>11</sub> OH	88.15	0.1798	-0.5847
C <sub>7</sub> H <sub>16</sub>	100.2	0.2434	-1.332

TABLE III: Volume Fractions Estimated from Mixing Conditions (Table I) and Moieties (Table II)

deuterated samples	micellar core	micellar core + Stern layer	
		50% pentanol in Stern layer	100% pentanol in Stern layer
TPB1	0.040	0.068	0.084
TPB3	0.084	0.111	0.126
TBP5	0.135	0.161	0.174
TBP7	0.185	0.208	0.221

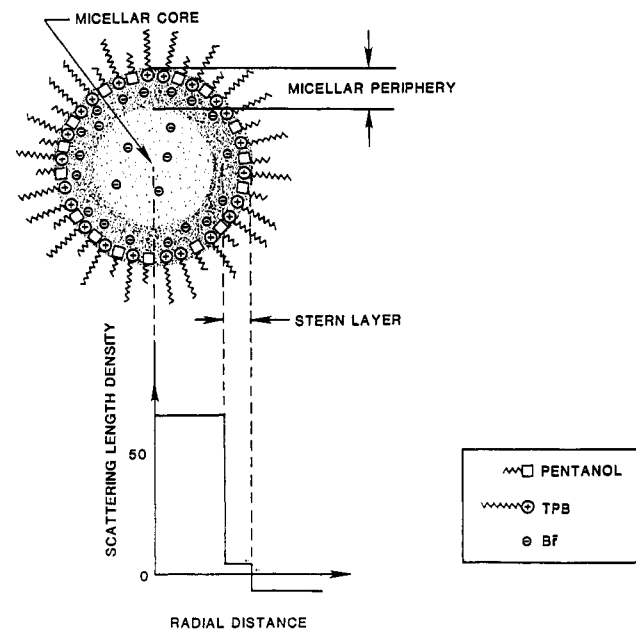


Figure 3. Scattering length densities in the micellar core, the Stern layer, and the outside hydrocarbon continuum.

intensity on the scattering vector  $Q$  for TPB12 is indicative of scattering from single particles, while the broadly peaked behavior of the ensuing samples is evidence of interference scattering when interparticle distances become comparable to particle sizes. The magnitude of the interparticle interactions can be seen to increase with increasing water concentration.

Estimates of the partial volumes of head groups, counterions, water molecules, and hydrocarbon subunits have been performed (Table II) to obtain estimated scattering volumes (Table III) based upon the mixing conditions of the samples. The average volumes for CH<sub>2</sub> and CH<sub>3</sub> were determined from the densities of pentane, hexane, heptane, and octane with relative standard deviations of 2.76% and 11.38%, respectively. Venable and Nauman<sup>22</sup> have determined via light-scattering and surface tension measurements that the trimethylammonium and pyridinium head groups occupy about the same area. The volume of the trimethylammonium head group was calculated from the literature<sup>23</sup> value of the cetyltrimethylammonium monomer volume, and the assumption was made that the volumes of the two head groups are approximately the same.

(22) Venable, R. L.; Nauman, R. V. *J. Phys. Chem.* **1964**, *68*, 3498.

(23) Farinato, R. S.; Rowell, R. L. *Solution Chemistry of Surfactants*; Plenum Press: New York, 1979; Vol. 2, p 311.

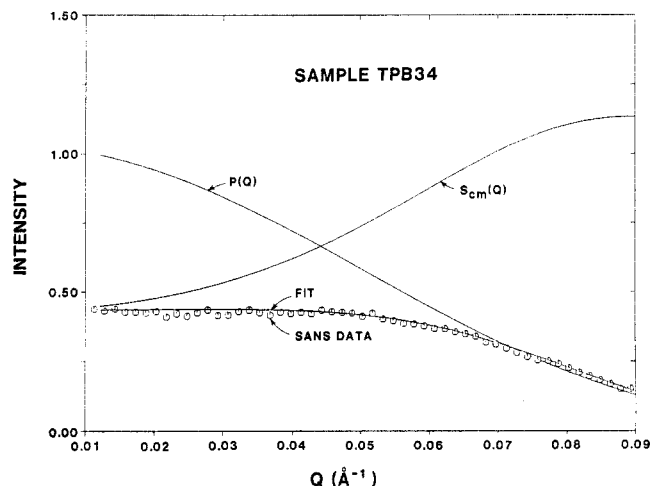


Figure 4. Result of the nonlinear least-squares fit (eq 4) for sample TPB34.  $P(Q)$  and  $S_{cm}(Q)$  are also plotted.

TABLE IV: Results of the Least-Squares Fit to Eq 4

sample	intercept	av radius $R$ , <sup>a</sup> Å	vol fraction $\eta$	droplet radius $r$ , Å
TBP12	59	18	0.00	
TPB34	1029	33	0.11	16
TPB56	5494	46	0.16	25
TPB78	16528	60	0.18	34

<sup>a</sup>The average radius  $R$  extracted from the Percus-Yevick fit represents an average intermicellar (center-to-center) distance.

The micellar model depicted in Figure 3 was used in conjunction with the estimated volumes to calculate scattering volumes (Table III) and scattering length densities. Moreover, we have assumed in the model that 77% of the bromide counterions are bound to

the Stern layer at a given time (with the other 23% distributed throughout the micellar core)<sup>24</sup> and that all the surfactant is located at the interface with a 50/50 partitioning of the alcohol between the interface and the continuous phase. Assuming 50% of the alcohol at the interface in the low water case gives a volume fraction of 6.8%, while assuming 100% of the alcohol residing at the interface would give a volume fraction of 8.4%, a difference of less than 2% (see Table III).

Calculations of the scattering length densities show (see Figure 3) that the main inhomogeneity visible to neutrons corresponds to the micellar core (heavy water with a fraction of the bromide counterions) along with the Stern layer (pyridinium head groups, a fraction of the pentanol head groups, and the remaining fraction of the bromide counterions) with a high coherent scattering cross section in a continuum of low scattering cross section (heptane, TPB tails, and pentanol tails and the remaining pentanol fraction dissolved in the oil phase).

Results of the fits of the corrected data (TPB12, 34, 56, 78) to eq 4 are included in Table IV. Figure 4 shows an example of such a fit for run TBP34 along with the single-particle  $P(Q)$  and interparticle  $S_{cm}(Q)$  structure factors. Comparisons of the measured volume fractions given in Table IV with the estimated values given in Table III show that the spherical micelles assumption is realistic and intermicellar interactions are fairly well screened (hard-sphere interactions).

*Acknowledgment.* Technical assistance from David Bradford, Jai Woo Chang, and Donald W. Mueller is greatly appreciated. This project has been partially supported by MURR funds.

**Registry No.** TPB, 1155-74-4; 1-pentanol, 71-41-0; *n*-heptane, 142-82-5.

(24) Ingram, T.; Jones, M. N. *Trans. Faraday Soc.* **1969**, *65*, 297.

## Negative Ion Formation from $N_2O$ Clusters by Impact of Highly Excited Rydberg Krypton Atoms and Electrons

Seiji Yamamoto, Koichiro Mitsuke,<sup>†</sup> Fuminori Misaizu,<sup>‡</sup> Tamotsu Kondow,<sup>\*</sup> and Kozo Kuchitsu<sup>§</sup>

Department of Chemistry, Faculty of Science, The University of Tokyo, Bunkyo-ku, Tokyo 113, Japan  
(Received: January 16, 1990; In Final Form: May 30, 1990)

Neutral clusters of nitrous oxide,  $(N_2O)_m$ , formed in a supersonic nozzle expansion were ionized by impact of high-Rydberg krypton atoms,  $Kr^{**}$ , and slow electrons having kinetic energies of 1–10 eV. Negative cluster ions,  $(N_2O)_nO^-$  ( $n \geq 3$ ) and  $(N_2O)_n^-$  ( $n \geq 5$ ), were produced by  $Kr^{**}$  impact, while  $(N_2O)_nO^-$  ( $n \geq 0$ ) and trace amounts of  $(N_2O)_nNO^-$  ( $n \geq 0$ ) and  $(N_2O)_n^-$  ( $n \geq 1$ ) were observed by electron impact. The intensity ratio,  $(N_2O)_n^- / (N_2O)_nO^-$ , produced by  $Kr^{**}$  impact was 2 orders of magnitude larger than that by electron impact. These observations are interpreted as follows: The  $(N_2O)_nO^-$  ions observed in both cases are produced via the  $N_2O^-(^2\Sigma^+)(N_2O)_{m-1}$  resonance state, where the  $N_2O^-(^2\Sigma^+)$  unit is solvated by the rest of the molecules. In the  $Kr^{**}$  impact ionization, several  $N_2O$  molecules are evaporated after dissociation of  $N_2O^-(^2\Sigma^+)(N_2O)_{m-1}$  into  $(N_2O)_{m-1}O^- + N_2$ . Formation of  $(N_2O)_n^-$  by  $Kr^{**}$  impact proceeds via the  $N_2O^-(^2\Pi)(N_2O)_{m-1}$  resonance state followed by substantial evaporation of  $N_2O$ . In contrast, intracuster ion-molecule reactions in  $(N_2O)_{m-1}O^-$  originating from  $N_2O^-(^2\Sigma^+)(N_2O)_{m-1}$  give rise to  $(N_2O)_nNO^-$  and  $(N_2O)_n^-$  observed by EI.

### Introduction

It is well-known that a nitrous oxide molecule,  $N_2O$ , captures an electron and dissociates into  $N_2$  and  $O^-$  (dissociative electron attachment).<sup>1-4</sup> The dissociation limit is located at only  $\sim 0.2$

eV above the neutral  $N_2O$ . Schulz<sup>1</sup> has shown by using trapped electron spectroscopy that the dissociative attachment proceeds via the resonance state having  $^2\Sigma^+$  symmetry which is located at 2.23 eV above the vacuum level. Later, Chantry<sup>2</sup> and Bardsley<sup>3</sup>

<sup>†</sup>Institute of Chemistry, The College of Arts and Sciences, The University of Tokyo, Komaba, Meguro-ku, Tokyo 153, Japan.

<sup>‡</sup>Institute for Molecular Science, Myodaiji, Okazaki 444, Japan.

<sup>§</sup>Department of Chemistry, Nagaoka University of Technology, Nagaoka 940-21, Japan.

(1) Schulz, G. J. *J. Chem. Phys.* **1961**, *34*, 1778.

(2) Chantry, P. J. *J. Chem. Phys.* **1969**, *51*, 3369.

(3) Bardsley, J. N. *J. Chem. Phys.* **1969**, *51*, 3384.

(4) Hopper, D. G.; Wahl, A. C.; Wu, R. L. C.; Tiernan, T. O. *J. Chem. Phys.* **1976**, *65*, 5474.